Real-Time Multi-Gigabit Receiver for Coherent Optical MIMO-OFDM Signals

Simin Chen, Qi Yang, Yiran Ma, and William Shieh

***Abstract*—In this paper we implement a first multi-gigabit real-time dual-polarization CO-OFDM receiver in a 2×2 multiple-input multiple-output (MIMO) configuration. The experimental setup consists of four 1.5 Giga samples per second (GS/s) high-speed analog-to-digital converters (ADC) and one Stratix III field-programmable gate array (FPGA). The signal streams are processed in real-time mode, and the data rates of 3.33 Gb/s and 6.67 Gb/s are realized for 4-QAM and 16-QAM, respectively.**

***Index Terms*—Coherent communications, field programmable gate array, multiple-input multiple-output, orthogonal frequency-division multiplexing, polarization diversity, quadrature amplitude modulation.**

I. Introduction

SINCE its short conception [1], coherent optical OFDM (CO-OFDM) has experienced rapid progress highlighted by the recent long-haul 100 Gb/s transmission from various groups [2]–[4]. CO-OFDM has been shown to combat chromatic dispersion [2]–[4] and polarization-mode dispersion [5], [6] and achieve high spectral efficiency [7] for the optical communication systems. However, all the above mentioned experiments are performed offline, and thus it would be of great interests to realize CO-OFDM in real-time. Recently, we reported the first multi-gigabit real-time CO-OFDM experiment with single-polarization [8]. As has been shown in [5], single-mode fiber (SMF) link in essence can be represented in a 2×2 multiple-input multiple-output (MIMO) channel, and some sort of polarization diversity, either transmit or receive diversity should be employed for practical implementation. On the other hand, with the rapid advance in silicon digital signal processing fuelled by the Moore's law, the high-speed analog-to-digital converter (ADC) at multi-gigahertz sampling rate and high-speed large-volume 40-nm field-programmable gate array (FPGA) are now commercially available. The sampled data can be transported into FPGAs through high-speed input/output (IO) interfaces such as low-voltage differential signalling (LVDS) for real-time processing. One of the advantages of the state-of-the-art FPGA is that it has sufficient gate resource, embedded memory and DSP blocks to process a digital signal in multiple parallel channels, allowing for a high-speed signal processed at a relatively lower clock rate. FPGA-based real-time optical transmission has been already demonstrated [9]–[11], and more impressive real-time 40 Gb/s system based on CMOS ASICs [12] has also been reported in single-carrier systems. In this paper, we show the first multi-gigabit real-time CO-OFDM receiver for dual polarizations in a 2×2 MIMO-OFDM configuration. The experimental setup consists of four 1.5 GS/s high-speed ADCs and one Stratix III FPGA. The signal streams are processed in real-time mode, and the net data rates of 3.33 Gb/s and 6.67 Gb/s are realized respectively for 4-QAM and 16-QAM modulations. To the best of our knowledge, this is the record real-time data rate for coherent OFDM reception, in either RF domain or optical domain.

This paper is organized as follows. In Section II, the principle of coherent optical MIMO-OFDM (CO-MIMO-OFDM) is presented. The experimental setup is described in Section III. In Section IV, we demonstrate the signal processing procedures and the algorithms used in the experiment. In Section V, we discuss the experimental results with a focus on BER performance. Finally, in Section VI we draw the conclusions.

II. Principal of Coherent Optical MIMO-OFDM

It is well-known that an SMF fiber can support two polarization modes. Propagation of an optical signal is influenced by polarization effects including polarization mode coupling and polarization dependent loss (PDL). This section will lay out the analytical derivation of linear effects including polarization mode dispersion (PMD) and chromatic dispersion (CD).

Similar to single-polarization OFDM signal model, the transmitted OFDM time-domain signal $\mathbf{s}(t)$ is described using Jones vector given by [5]

$$\mathbf{s}(t) = \sum_{i=-\infty}^{+\infty} \sum_{k=-(1/2)N_{sc}+1}^{1/2N_{sc}} \mathbf{c}_{ik} \prod(t - iT_s) \times \exp(j2\pi f_k(t - iT_s)) \quad (1)$$

$$\mathbf{s}(t) = \begin{bmatrix} s_x \\ s_y \end{bmatrix}, \quad \mathbf{c}_{ik} = \begin{bmatrix} c_{ik}^x \\ c_{ik}^y \end{bmatrix} \quad (2)$$

$$f_k = \frac{k-1}{t_s} \quad (3)$$

$$\prod(t) = \begin{cases} 1, & (-\Delta_G < t < t_s) \\ 0, & (t \le -\Delta_G, t > t_s) \end{cases} \quad (4)$$

where s_x and s_y are the two polarization components for $\mathbf{s}(t)$ in time-domain, $\mathbf{c}_{ik}$ represents the transmitted OFDM symbol in the form of Jones vector for the kth subcarrier in the ith OFDM symbol, c_{ik}^x and c_{ik}^y are the two polarization components of $\mathbf{c}_{ik}$. f_k is the frequency for the kth subcarrier, N_{sc} is the number of OFDM subcarriers, T_s, Δ_G, and t_s are the OFDM symbol period, guard interval length and observation period respectively. Bold font convention is used to represent a vector or matrix. The

Manuscript received January 15, 2009; revised May 04, 2009.

S. Chen and W. Shieh are with the ARC Special Research Centre for Ultra-Broadband Information Networks, Department of Electrical and Electronics Engineering, University of Melbourne, Melbourne, VIC 3010, Australia (e-mail: siminc@ee.unimelb.edu.au; w.shieh@ee.unimelb.edu.au).

Q. Yang and Y. Ma are with the Victoria Research Laboratory, National ICT Australia, Department of Electrical and Electronic Engineering, University of Melbourne, Melbourne, VIC 3010, Australia (e-mail: q.yang@ee.unimelb.edu.au; yiranm@ee.unimelb.edu.au).

Color versions of one or more of the figures in this paper are available online at http://ieeexplore.ieee.org.

Digital Object Identifier 10.1109/JLT.2009.2023340

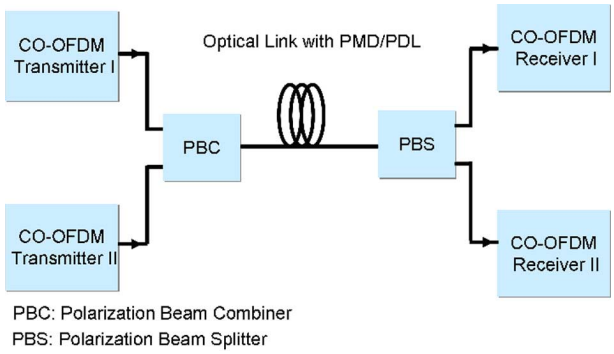

Fig. 1. Coherent optical MIMO-OFDM model.

Jones vector $\mathbf{c}_{ik}$ is employed to describe generic OFDM information symbol regardless of any polarization configuration for the OFDM transmitter.

The guard interval should be long-enough to handle the fiber dispersion including PMD and CD. This timing margin condition is given by

$$\frac{c}{f^2}|D_t| \cdot N_{sc} \cdot \Delta f + DGD_{\max} \le \Delta_G \tag{5}$$

where f is the frequency of the optical carrier, c is the speed of light, D_t is the total accumulated chromatic dispersion in units of ps/km, N_{sc} is the number of the subcarriers, Δf is the subcarrier channel spacing, and $DGD_{\max}$ is the maximum budgeted differential-group-delay (DGD), which is about 3.5 times of the mean PMD to have sufficient margin.

Following the same procedure as [1], assuming using long-enough symbol period, the received signal is given by

$$\mathbf{c}'_{ik} = e^{j\phi_i} \cdot e^{j\Phi_D(f_k)} \cdot \mathbf{T}_k \cdot \mathbf{c}_{ik} + \mathbf{n}_{ik} \tag{6}$$

$$\Phi_D(f_k) = \frac{\pi \cdot c \cdot D_t \cdot f_k^2}{f_{LD1}^2} \tag{7}$$

where $\mathbf{c}'_{ik} = [c'^x_{ik} \quad c'^y_{ik}]^T$ is the received information symbol in the form of the Jones vector for the kth subcarrier in the ith OFDM symbol, superscript 'T' represents the matrix transpose, $\mathbf{n}_{ik} = [n^x_{ik} \quad n^y_{ik}]^T$ is the noise including two polarization operator, T_k is the Jones matrix for the fiber link, $\Phi_D(f_k)$ is the phase dispersion owing to the fiber chromatic dispersion [1], and ϕ_i is the OFDM common phase error (CPE) owing to the phase noises from the lasers and RF local oscillators (LO) at both the transmitter and receiver [1].

The expression (6) can be presented in an equivalent MIMO-OFDM model, with both a polarization-diversity transmitter and a polarization-diversity receiver are employed in the 2×2 MIMO scheme as shown in Fig. 1. Because the transmitted OFDM information symbol $\mathbf{c}_{ik}$ can be considered as polarization modulation or polarization multiplexing, the capacity is thus doubled compared with single polarization scheme. As the impact of PMD is to simply rotate the subcarrier polarization and can be treated with channel estimation, therefore the doubling of channel capacity will not be affected by PMD. Besides, due to the polarization-diversity receiver employed at the receive end, MIMO scheme does not need polarization tracking at the receiver. The enormous dispersion capability of the OFDM lies in the fact that as long as a sufficiently large guard interval is used as shown by (5), the inter-symbol interference (ISI) is effectively avoided. In this paper, we focus on the real-time digital signal processing of 2×2 MIMO-OFDM for dual-polarization data recovery. The optical dispersion aspect of a real-time CO-OFDM receiver will be shown in a separate ensuing submission.

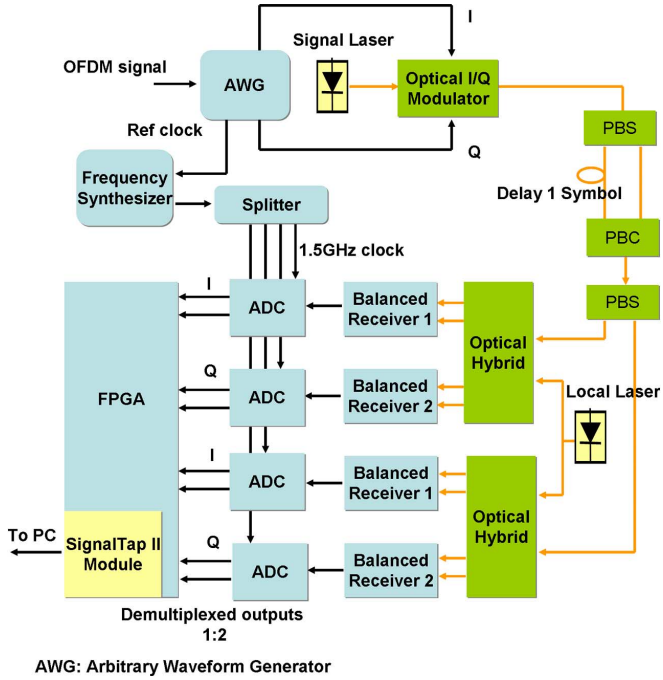

Fig. 2. Experimental setup for real-time reception of coherent optical MIMO-OFDM signals.

III. Experimental Setup

In this section, we will describe essential devices and components for the real-time 2×2 MIMO-OFDM receiver platform. Fig. 2 shows the experimental setup incorporating the real-time CO-OFDM receiver for dual polarizations in a 2×2 MIMO-OFDM configuration. The transmitted signal is generated by MATLAB program originated from $2^{15} - 1$ pseudo random binary sequence (PRBS), and then mapped to 4-QAM or 16-QAM data symbols. The time domain signal is formed after inverse fast Fourier transform (IFFT) operation, and then inserted with guard interval. The I and Q components of the time-domain OFDM signal is uploaded onto Tektronix Arbitrary Waveform Generator (AWG), which produces the analog signals at 1.5 GS/s. Total number of OFDM subcarriers is 64; Guard interval is 1/8 observation window; 48 subcarriers out of 64 are filled; 4 of them are used for phase estimation; 32 out of 500 OFDM symbols are used as training symbols for channel estimation. The number of training symbols can be reduced to take advantage of the frequency domain correlation of channel transfer function [14]. An optical I/Q modulator comprised of two Mach–Zehnder modulators (MZM) with 90° phase shift, directly up-converts OFDM baseband signals from the RF domain to the optical domain. The single-polarization optical OFDM signal at the output of the I/Q modulator is then evenly split into two polarization branches via a polarization-beam splitter (PBS), with one branch delayed by one OFDM symbol period, i.e., 48 ns in this experiment. The two polarization branches are subsequently combined by a polarization-beam combiner (PBC), emulating two independent transmitters, one for each polarization, resulting in a composite raw data rate of 1.92 Gb/s for 4-QAM and 3.83 Gb/s for 16-QAM. The net data rate is

1.67 Gb/s for 4-QAM and 3.33 Gb/s for 16-QAM after excluding the overhead from cyclic prefix and pilot tones.

At the receiver side, direct optical-to-RF down-conversion is employed. We tune the LO laser frequency close to that of the incoming signal. The tolerance of frequency difference between signal laser and local laser is ± 2 subcarrier spacings, which is determined by the frequency synchronization algorithm. The optical signal is fed into a PBS for a polarization diversity coherent receiver. Each branch of the splitter is mixed with a local laser with an optical 90° hybrid, and I and Q ports from the optical 90° hybrid are used for direct down-conversion. Two balanced receivers at each branch are used to detect I and Q components. The RF signals from the four balanced detectors are firstly passed through antialiasing low-pass filters with a bandwidth of 575 MHz, such that only a small portion of the frequency components beyond signal bands is passed through. The detected RF signals are then sampled with four high-speed E2V ADCs at 1.5 GS/s. Then the signals are transmitted via LVDS interface into Altera Stratix III FPGA through 1:2 demultiplexed outputs, which lowers the rate down to 750 MS/s. Multiple inputs are received and de-multiplexed into 8 channels at 187.5 Ms/s in the FPGA for further signal processing. After all the OFDM signal processing, the recovered data are compared with the transmitted ones in FPGA and errors are counted. This error count, together with transmitted OFDM symbol numbers, is then sampled by SignalTap II debugging module and transported via a JTAG cable to PC for BER collection.

A frequency synthesizer is used to receive 10 MHz reference clock from AWG and generate 1.5 GHz sampling clock for four ADCs. FPGA is driven by a 375 MHz clock from one ADC which is derived from its sampling clock input and this clock is then further divided down to 187.5 MHz by embedded phase-locked loop (PLL) to act as the major clock source for the receiver. As such, the clocks in the receiver system are completely synchronized.

In the experiment, we use synchronized clocks to simplify the experiment that is focused on CO-OFDM algorithm implementations. The sampling clock offset is an important problem and has been well treated previously [16]. In practice, such restriction can be avoided by adding a digital phase lock loop (DPLL) module at the receiver in the FPGA that can feed back the error signal to adjust the sampling clock of the ADCs. In doing so, the physical clock link from transmitter to receiver can be released.

IV. Signal Processing Algorithms

The CO-MIMO-OFDM receiver architecture is divided into nine stages: (1) timing synchronization, (2) frequency synchronization, (3) CP removal to recover OFDM block, (4) FFT to recover the frequency-domain symbols, (5) phase estimation for training symbols, (6) channel estimation, (7) Jones matrix inversion to recover two polarization signals, (8) phase estimation for payload symbols, (9) symbol decision, error accumulation and BER computation. Some important stages of signal processing are discussed in detail below:

(1) Timing synchronization. In this stage, the OFDM symbol is properly delineated to avoid inter-symbol interference. The most popular pilot-aided algorithm is the one proposed by Schmidl [14]. His method uses a training symbol with the same two identical halves to estimate the symbol timing and frequency offset. However the timing metric of this method has a plateau that causes timing uncertainty. In this experiment we use a new form of time-domain preamble [15] that is partitioned into four segments as

$$P = [\, A_{N/4} \quad A_{N/4} \quad A_{N/4} \quad -A_{N/4} \,]$$

where $A_{N/4}$ represents samples of length $N/4$ generated by IFFT of a PN sequence.
The timing metric is expressed as

$$M(d) = \frac{|P(d)|^2}{(R(d))^2} \tag{8}$$

where

$$\begin{aligned} P(d) = & \sum_{k=0}^{N/4-1} r^*(d+k) r\left(d+k+\frac{N}{4}\right) \\ & + \sum_{k=0}^{N/4-1} r^*\left(d+k+\frac{N}{4}\right) r\left(d+k+\frac{N}{2}\right) \\ & - \sum_{k=0}^{N/4-1} r^*\left(d+k+\frac{N}{2}\right) r\left(d+k+\frac{3N}{4}\right) \end{aligned} \tag{9}$$

$$R(d) = \sum_{m=0}^{3} \sum_{k=0}^{N/4-1} \left| r\left(d+k+m\frac{N}{4}\right) \right|^2. \tag{10}$$

This timing metric has its peak at the correct starting point of OFDM symbol. That is

$$d_i = \arg\{\max[M(d)]\} \tag{11}$$

where d_i stands for the optimal timing metric. The timing metric of real-time data is shown in Fig. 3. It can be seen that the peak of timing metric is sharp and obvious, signifying that the timing estimation is accurate.

(2) Frequency synchronization. Frequency offset between signal laser and local laser must be estimated and compensated before further processing. The algorithm used in this stage is similar to Schmidl's [14], expressed as

$$\hat{\phi} = angle(P(d)). \tag{12}$$

Once the frequency offset is estimated, the received sampled signal will be compensated as

$$r_c(t) = \exp\left(\frac{-j \cdot 2\pi \cdot \hat{\phi} \cdot t}{\left(\frac{N}{4}\right)}\right) \cdot r(t). \tag{13}$$

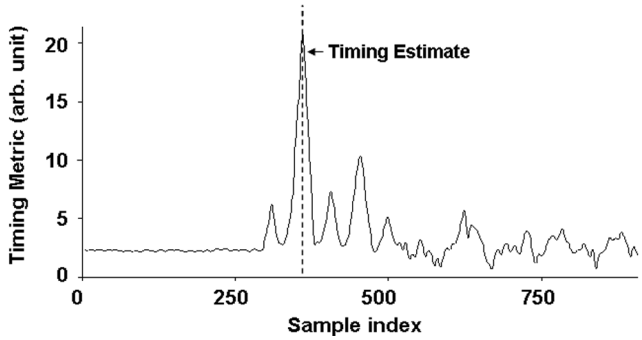

Fig. 3. Timing metric for the CO-OFDM signal.

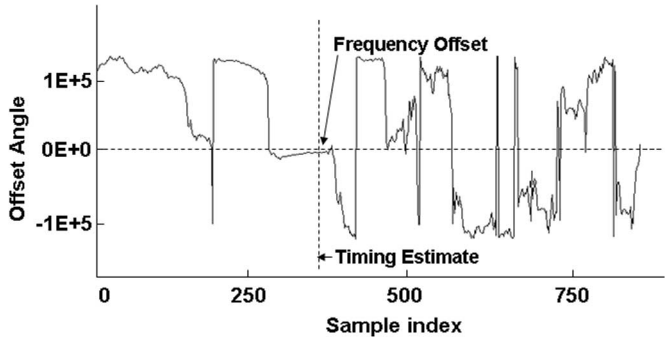

Fig. 4. Frequency offset estimate for the CO-OFDM signal.

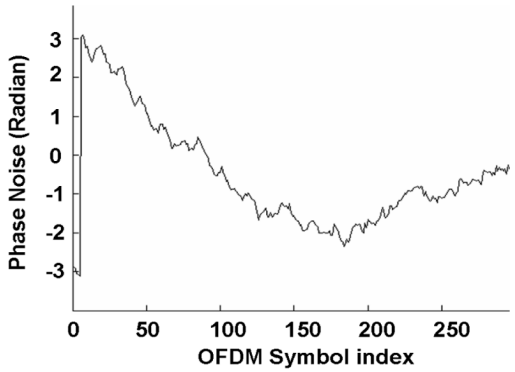

Fig. 5. Estimated common phase error (CPE) as a function of CO-OFDM symbol sequence.

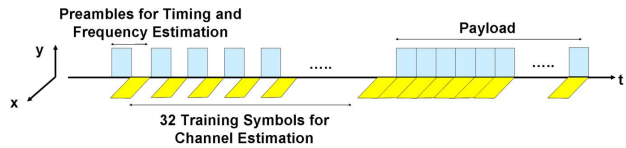

Fig. 6. Time-domain representation of the dual-polarization OFDM block including training symbols for timing and frequency synchronization, channel estimation, and payload. 'x ' and 'y' represent two polarization components.

Coordinate Rotation Digital Computer (CORDIC) algorithm is used to calculate the frequency offset angle and compensate input data in vectoring mode and rotation mode respectively. Fig. 4 shows the frequency offset angle output. As 18-bit resolution is used, the output range is from -131072 to 131071, corresponding to the actual angle range from $-\pi$ to π. Once the signal of timing estimate from timing synchronization stage is detected, the current output value of $\hat{\phi}$ is the correct frequency offset as shown in Fig. 4.

(3) Phase estimation for training symbols and payload symbols. The phase estimation is to obtain the CPE ϕ_i due to the laser phase noise. We assume that N_p pilot subcarriers are used for phase estimation, and the maximum likelihood CPE can be estimated as [17]

$$\phi_i = angle\left(\sum_{k=1}^{N_p} r_{ki} h_k^* c_{ki}^*\right) \tag{14}$$

where

$$h_k = \sum_{i=1}^{N_p} \frac{e^{-j\angle r_{k_1 i}} r_{ki}}{c_{ki}} \tag{15}$$

r_{ki} and c_{ki} are received and transmitted pilot subcarrier symbols respectively. $\angle r_{k_1 i}$ is the angle for the k_1th carrier (an arbitrary reference carrier) in the ith OFDM symbol. N_p is the number of pilot symbols and c_{ki}^* represents the conjugate of transmitted symbol. The additional phase compensation of -$\angle r_{k_1 i}$ is needed to remove the influence of the common phase error.

In real-time implementation, division operation takes much more resources and clock cycles to perform than multiplication. From (14) and (15), it can be seen that only the phase difference between the transmitted and received subcarriers determines CPEϕ_i, and therefore division of r_{ki}/c_{ki} in (15) is replaced with multiplication of $r_{ki} \cdot c_{ki}^*$ to simplify the computation.

The estimated phase ϕ_i will be used to de-rotate the received pilot symbols for the channel estimation to obtain channel transfer function $\boldsymbol{H}$. The estimated phase ϕ_i is also used to de-rotate the recovered data symbols and subsequently de-mapped to the closest symbol to recover the transmitted data [5].

Fig. 5 shows the calculated phase noise as a function of OFDM symbol index. The abrupt phase jump at the beginning of figure is due to the 2π phase wrap.

(4) Channel estimation. The channel matrix $\boldsymbol{H}$ is estimated by sending 32 OFDM symbols using alternative polarization launch. The total number of OFDM symbol evaluated is 500 symbols. Although minimum mean-squared-error (MMSE) channel estimation algorithm achieves better performance than zero forcing (ZF), it requires higher computational complexity and larger chip resource consumption. In this experiment ZF algorithm is used. Efficient implementation of MMSE scheme is left for further research in the future.

Mathematically, the transmitted data symbol of the two polarizations in the forms of Jones vector are given by

$$\mathbf{c} = \begin{bmatrix} c_x \\ c_y \end{bmatrix}. \tag{16}$$

Assume the fiber transmission Jones matrix $\boldsymbol{H}$ is

$$\mathbf{H} = e^{j\Phi_D(f_k)} \cdot \mathbf{T}_k = \begin{bmatrix} h_{xx} & h_{xy} \\ h_{yx} & h_{yy} \end{bmatrix}. \tag{17}$$

From (6), the two received scalar OFDM symbols c_x' and c_y' after the phase estimation and compensation are

$$\begin{cases} c_x' = h_{xx} c_x + h_{xy} c_y + n_x \\ c_y' = h_{yx} c_x + h_{yy} c_y + n_y \end{cases} \tag{18}$$

where n_x and n_y are the random noises for two polarizations. We have dropped the subcarrier index k and OFDM symbol index i for the sake of simplicity in (18). From the expression (18), the transmitted data symbols can be recovered from the received signals by inverting H:

$$\mathbf{c} = \mathbf{H}' \begin{bmatrix} c_x' \\ c_y' \end{bmatrix} + \mathbf{H}' \begin{bmatrix} n_x \\ n_y \end{bmatrix}, \quad \mathbf{H}' = \begin{bmatrix} h_{xx} & h_{xy} \\ h_{yx} & h_{yy} \end{bmatrix}^{-1}. \tag{19}$$

Subsequently the estimated transmitted symbol, $\hat{\mathbf{c}}$ is given by

$$\hat{\mathbf{c}} = \begin{bmatrix} \hat{c}_x \\ \hat{c}_y \end{bmatrix} = \mathbf{H}' \begin{bmatrix} c_x' \\ c_y' \end{bmatrix} \tag{20}$$

$\hat{c}_x$ and $\hat{c}_y$ are the estimated transmitted symbols encoded onto the two polarizations and will be subsequently de-mapped to the nearest constellation points to recover the transmitted symbols.

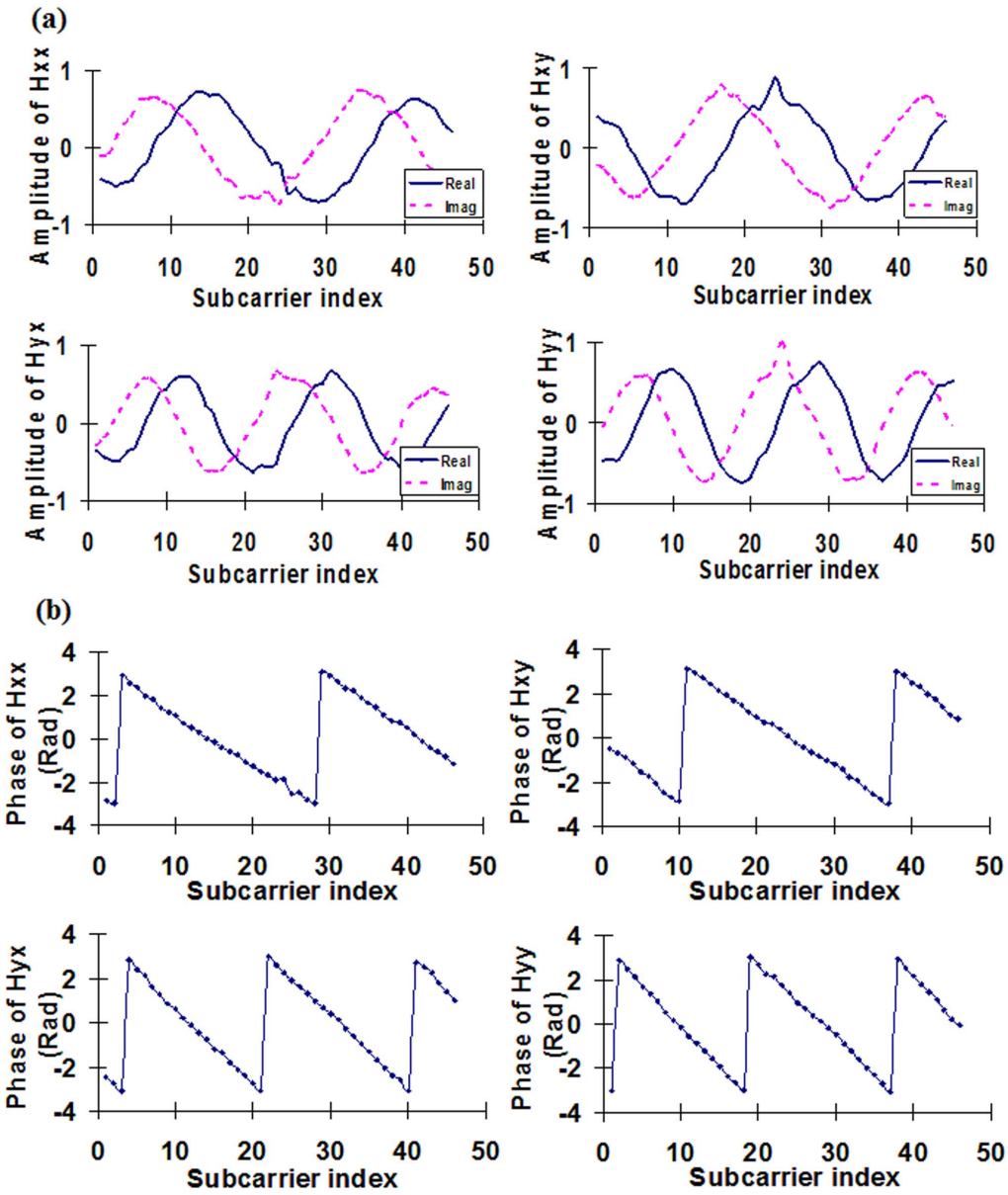

Fig. 7. (a) Amplitude and (b) phase of estimated channel transfer function matrix elements H_{xx}, H_{xy}, H_{yx} and H_{yy} as a function of subcarrier index.

The training symbols are generated by filling the odd symbols with normal transmitted data, while leaving the even symbols blank. After the polarization multiplexing emulator, the training symbols form a pattern of alternative polarization launch for two consecutive OFDM symbols as depicted in Fig. 6. Using odd training symbols, channel estimation can be expressed as

$$\begin{bmatrix} c'_x \\ c'_y \end{bmatrix} = \begin{bmatrix} h_{xx} & h_{xy} \\ h_{yx} & h_{yy} \end{bmatrix} \begin{bmatrix} c_x \\ 0 \end{bmatrix} \Rightarrow \begin{cases} h_{xx} = \frac{c'_x}{c_x} \\ h_{yx} = \frac{c'_y}{c_x} \end{cases} \tag{21}$$

and using even training symbols as

$$\begin{cases} h_{xy} = \frac{c'_x}{c_y} \\ h_{yy} = \frac{c'_y}{c_y}. \end{cases} \tag{22}$$

It can be seen from (21) and (22), by using alternative polarization training symbol, the full channel estimation of $\boldsymbol{H}$ can be obtained. The results of matrix $\boldsymbol{H}$ are plotted in Fig. 7(a) and (b). The abrupt phase jump in Fig. 7(b) is due to the 2π phase wrap. The subcarrier index range is 1 to 48 because 48 out of 64 subcarriers are used. Then using the inverse of this matrix in (20) and the received data symbols, the transmitted symbols in the two polarizations can be estimated.

V. Measurement and Discussion

The real-time MIMO-CO-OFDM receiver uses a resource of 28% of Look-Up Table (LUT), 35% of dedicated registers, 26% of memory and 48% of DSP blocks of the FPGA chip (Altera Stratix III EP3SL340H1152). Fig. 8 shows the BER performance of 3.33 Gb/s 4-QAM and 6.67 Gb/s 16-QAM coherent optical MIMO-OFDM signals at back-to-back transmission comparing with that of single polarization CO-OFDM reported in [8]. Each point in this figure is an average of 50 OFDM transmission blocks each containing 288 OFDM data symbols. The combined laser linewidth is about 100 kHz. A BER of 10^{-3} can be observed at an OSNR of 0.6 dB (ASE noise bandwidth of 0.1 nm) for 4-QAM signal with the polarization dependence less than 0.3 dB. The OSNR requirement for 4-QAM MIMO transmission increases

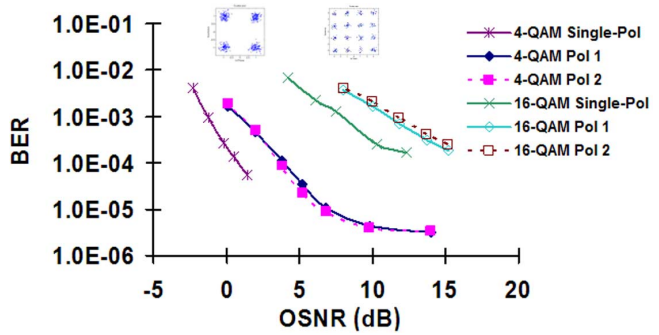

Fig. 8. Real-time BER performance for CO-OFDM signal at back-to-back transmission. Constellations for 4-QAM and 16-QAM are measured at 5 dB and 14.8 dB OSNR, respectively.

by 2.7 dB at 10^{-3} BER compared with single polarization, which is close to the theoretical penalty of 3 dB. A BER floor emerges at around 3×10^{-6} because the training symbol length is only 64 points, which limits the accuracy of frequency offset estimation. The obtained data rate is limited to 3.33 Gb/s due to the maximum sampling rate of 1.5 GS/s offered by the ADCs used. The choice of only filling 46 subcarriers out of 64 is due to 575 MHz antialias filter used. Accessing a higher sampling rate ADCs can further improve the data rate. We also show the performance of 6.67 Gb/s 16-QAM in Fig. 8. The OSNR sensitivity for a BER of 10^{-3} is about 11 dB. The relative large penalty compared to the 4-QAM is due to the BER floor at 10^{-4}. This BER floor for 16-QAM is attributed to the limited 7-bit resolution, and large phase drift due to long OFDM symbol length by using relatively low sampling rate of 1.5 GS/s. This can be avoided to use ADC with higher sampling rate. Nevertheless, our demonstration has achieved a record data rate of 6.67 Gb/s for real-time reception of coherent OFDM signals, in either RF domain or optical domain. The insets in Fig. 8 show the constellation diagrams for received 4-QAM and 16-QAM CO-OFDM signals indicating the successful operation of the real-time signal processing.

VI. Conclusion

In this paper we have demonstrated the first multi-gigabit real-time dual-polarization CO-OFDM receiver in a 2×2 multiple-input multiple-output (MIMO) configuration. The experimental setup consists of four 1.5 GS/s high-speed ADCs, and one Stratix III FPGA. A record data rate of 6.67 Gb/s is realized for coherent OFDM systems either in RF or optical domain.

References

[1] W. Shieh and C. Athaudage, "Coherent optical orthogonal frequency division multiplexing," *Electron. Lett.*, vol. 42, pp. 587–589, 2006.
[2] W. Shieh, Q. Yang, and Y. Ma, "107 Gb/s coherent optical OFDM transmission over 1000-km SSMF fiber using orthogonal band multiplexing," *Opt. Exp.*, vol. 16, pp. 6378–6386, 2008.
[3] E. Yamada, A. Sano, and H. Masuda, "1 Tb/s (111 Gb/s/ch $\times$ 10 ch) no-guard-interval CO-OFDM transmission over 2100 km DSF," presented at the OECC'2008, paper PDP 6.
[4] S. L. Jansen, I. Morita, and H. Tanaka, "10 $\times$ 121.9-Gb/s PDM-OFDM transmission with 2-b/s/Hz spectral efficiency over 1,000 km of SSMF," presented at the OFC'2008, paper PDP2.
[5] W. Shieh, X. Yi, Y. Ma, and Q. Yang, "Coherent optical OFDM: Has its time come?," *J. Opt. Netw.*, vol. 7, pp. 234–255, 2008.
[6] S. L. Jansen, I. Morita, and H. Tanaka, "16 $\times$ 52.5-Gb/s, 50-GHz spaced, POLMUX-CO-OFDM transmission over 4,160 km of SSMF enabled by MIMO processing KDDI R&D laboratories," presented at the ECOC, Berlin, Germany, 2007, paper PD1.3.
[7] X. Yi, W. Shieh, and Y. Ma, "Phase noise effects on high spectral efficiency coherent optical OFDM transmission," *J. Lightw. Technol.*, vol. 26, pp. 1309–1316, 2008.
[8] S. Chen, Q. Yang, Y. Ma, and W. Shieh, "Multi-gigabit real-time coherent optical OFDM receiver," presented at the OFC'2009, Paper OTuO4.
[9] T. Pfau, S. Hoffmann, R. Peveling, S. Bhandare, S. K. Ibrahim, O. Adamczyk, M. Porrmann, R. Noe, and Y. Achiam, "First real-time data recovery for synchronous QPSK transmission with standard DFB lasers," *IEEE Photon. Technol. Lett.*, vol. 18, pp. 1907–1909, 2006.
[10] A. Leven, N. Kaneda, and Y. K. Chen, "A real-time CMA-based 10 Gb/s polarization demultiplexing coherent receiver implemented in an FPGA," presented at the OFC 2008, Paper OTuO2.
[11] H. Song, A. Adamiecki, P. J. Winzer, C. Woodworth, S. Corteselli, and G. Raybon, "Multiplexing and DQPSK precoding of 10.7-Gb/s client signals to 107 Gb/s using an FPGA," presented at the OFC'2008, Paper OTuG3.
[12] H. Sun, K. Wu, and K. Roberts, "Real-time measurements of a 40 Gb/s coherent system," *Opt. Exp.*, vol. 16, pp. 873–879, 2008.
[13] X. Liu and F. Buchali, "Intra-symbol frequency-domain averaging based channel estimation for coherent optical OFDM," *Opt. Exp.*, vol. 16, pp. 21944–21957, 2008.
[14] T. M. Schmidl *et al.*, "Robust frequency and timing synchronization for OFDM," *IEEE Trans. Commun.*, vol. 45, pp. 1613–1621, 1997.
[15] H. Minn, V. K. Bhargava, and K. B. Letaief, "A robust timing and frequency synchronization for OFDM systems," *IEEE Trans. Wireless Commun.*, vol. 2, no. 4, pp. 822–839, 2003.
[16] T. Pollet, P. Spruyt, and M. Moeneclaey, "The BER performance of OFDM systems using non-synchronized sampling," *Proc. GLOBECOM '94*, pp. 253–257, 1994.
[17] W. Shieh, X. Yi, Y. Ma, and Q. Yang, "Coherent optical OFDM: Has its time come?," *J. Opt. Netw.*, vol. 7, pp. 234–255, 2008.

Simin Chen was born in Fujian, China. He received the B.S. and M.S. degree in electrical and electronic engineering both from Sichuan University, Chengdu, China. Currently he is working toward his Ph.D. degree in electrical and electronic engineering department at the University of Melbourne, Australia.

From 2006 to 2007 he worked in Fiberxon Inc. (acquired by MRV in 2007) on optical transiver and FPGA. His research interests include signal processing and coherent optical communication systems with a focus on the real-time implementation of coherent optical OFDM transmitter and receiver.

Qi Yang was born in Wuhan, China, in 1981. He received the B.E. and M.E. degrees in electronic and information engineering from Huazhong University of Science and Technology, Wuhan, China. Since February 2007, he has been studying as Ph.D student in electrical and electronic engineering from the University of Melbourne, Melbourne, Australia, where he specialized in CO-OFDM in long haul transmission

In 2006, he was at Huagong Genuine Optics Technology Co. Ltd. He was involved in optical CDMA module and system design. His main research interests are OFDM, coherent detection, and high speed system design.

Yiran Ma received the B.Eng. degree in telecommunication engineering in 2005 from the Harbin Institute of Technology, Harbin, China, the M.S. degree in telecommunications engineering degree from the University of Melbourne, Melbourne, Australia, where he is currently working toward the Ph.D. degree.

In 2005, he was an Intern for half a year at the China Academy of Space Technology, where he developed algorithms of real-time encryption and decryption for communication networks. His current research interests include coherent optical system design, signal processing of MIMO-OFDM, and nonlinearity in optical long-haul systems.

William Shieh (S'96–M'96) received the M.S. degree in electrical engineering-communications and the Ph.D. degree in physics from the University of Southern California, Los Angles, in 1994 and 1996, respectively.

From 1996 to 1998, he worked as a member of Technical Staff in the Jet Propulsion Laboratory, Pasadena, CA. From 1998 to 2000, he worked as a member of the Technical Staff in Bell Labs, Lucent Technologies, Holmdel, NJ. From 2000 to 2003, he worked as a Technical Manager in Dorsal Networks, Columbia, MD. Since 2004, he has been with the Department of Electrical and Electronic Engineering, University of Melbourne, Melbourne, Australia. His current research interests include OFDM techniques in both wireless and optical communications, coherent optical communication systems, and optical packet switching. He has published more than 80 journal and conference papers, and submitted 14 U.S. patents (nine issued) covering areas of polarization controller, wavelength stabilization in WDM systems, and Raman amplifier-based systems and subsystems.